Doping-induced antiferromagnetic bicollinear insulating state and superconducting temperature of monolayer FeSe systems

Michael C. Lucking, Fawei Zheng, Myung Joon Han, Junhyeok Bang, and Shengbai Zhang

Phys. Rev. B **98**, 014504 — Published 9 July 2018

DOI: 10.1103/PhysRevB.98.014504

Doping-Induced Antiferromagnetic Bicollinear Insulating State and Superconducting Temperature of Monolayer FeSe Systems

Michael C. Lucking,[1] Fawei Zheng,[2] Myung Joon Han,[3] Junhyeok Bang,[4*] and Shengbai Zhang[1*]

[1]*Department of Physics, Applied Physics & Astronomy, Rensselaer Polytechnic Institute, Troy, NY 12180, USA*

[2]*Institute of Applied Physics and Computational Mathematics, Beijing, 100088, China*

[3]*Department of Physics, Korea Advanced Institute of Science and Technology (KAIST), Daejeon 305-701, South Korea*

[4]*Spin Engineering Physics Team, Korea Basic Science Institute (KBSI), Daejeon 305-806, South Korea*

Abstract

First-principles calculations of ionic-liquid-gated (Li,Fe)OHFeSe suggest a metal-insulator transition at a nominal Li/Fe ratio of 75/25 in the (Li,Fe)OH layer. While doping increases Fermi energy, the formation of an antiferromagnetic bicollinear phase is the key for the transition. It is expected that this insulating phase also exists in other FeSe systems upon heavy electron doping, and its presence can hinder the increase of superconducting temperature. These results offer clues on how to optimize superconductivity amid its interplay with magnetic properties in FeSe systems.

[*]Corresponding authors: jbang0312@kbsi.re.kr and zhangs9@rpi.edu

The discovery of iron oxy-pnictide superconductor LaOFeP with a superconducting transition temperature T_C = 4 K [1] has laid the foundation for iron-based superconductivity. Not only are the materials non-ceramics, but also it contains ferromagnetic elements, i.e., iron, in spite of the incompatibleness between superconductivity and magnetism, which makes the iron-based materials exceptionally interesting. Within the iron-superconductor family, layered FeSe, with T_C = 8.5 K [2] in ambient pressure, has emerged as a subject of intense study, as a T_C as high as > 100 K [3] (which is more than tenfold of the bulk value) may be obtained by placing a monolayer (ML) FeSe on a $SrTiO_3$ (STO) substrate. This result is truly exceptional, as many experiments have shown that, even at the optimal condition, T_C of a FeSe-derived superconductors is in the neighborhood of or below 40 K, for examples, the highest T_C= 32 K for $K_xFe_{2-y}Se_2$ [4], 31 K for $(Tl,K)Fe_xSe_2$ [5], and 36.7 K for FeSe under pressure [6]. It hints for a unique mechanism of the superconductivity in the ML FeSe system. For example, recent experimental and theoretical studies showed that interfacial electron-phonon coupling may play a role for the significantly enhanced T_C [7-10].

As having been shown in cuprates and other Fe-based superconductors, the interplay between magnetism and superconductivity, as reflected in their phase diagrams, are sensitive to carrier doping and applied pressure. As such, the phase diagram holds the key to the understanding of the superconductivity. An interrogation of such an interplay in the FeSe systems is, however, hindered by the low stability and phase separation [11,12]. Recently, a new FeSe superconductor, (Li,Fe)OHFeSe, which can be viewed as a stack of ML FeSe separated by (Li,Fe)OH spacers [11-18], has emerged, which is suitable for the study of phase diagram by gate-tunable ionic liquid doping [12]. By this approach, T_C up to 43 K, which is similar to the highest T_C for other FeSe-derived superconductors, is observed. Unfortunately, however, a further increase of T_C by doping is hindered by the formation of an unknown antiferromagnetic (AFM) insulating phase. Alternatively, the AFM phase in (Li,Fe)OHFeSe may be related to the insulating phase of heavily-doped FeSe, which is a result of an electronic correlation effect [19]. In the heavily-doped ML FeSe on STO, on the other hand, T_C increases monotonically without such an insulating phase [20], whereby defying all the odds. One may, therefore, wonder if a further increase of T_C is indeed possible without invoking any unconventional superconductivity theory, when the formation of the AFM insulating phase can be suppressed.

In this paper, first-principles density functional theory (DFT) is used to study the mysterious AFM insulating phase, which is identified as the *bi*collinear (double-stripe) (BI) phase in (Li,Fe)OHFeSe. It becomes stable at a Li/Fe ratio of 75/25 in the (Li,Fe)OH layer, i.e., 0.25 electron/Fe doping at the FeSe layer, and is stabilized by an spin-phonon coupling to result in a large iron relaxation of 7% and Fe double-dimers. A phase diagram for (Li,Fe)OHFeSe is thus established: at low gate voltage, a ground-state AFM metallic collinear (CO) phase has the lowest energy, and the superconductivity can arise in close proximity to this AFM CO phase. As the gate voltage increases, the BI phase becomes stable. When the gate voltage increases further, the system transitions back to the CO phase, and finally to an insulating pair-checkerboard (PA) phase. The transition to BI phase by gate voltage is in qualitative agreement with available experiments [12]. The BI phase is expected to be stable in other heavily-doped FeSe systems, as well. Hence, one must avoid the BI phase in order to further increase T_C, as may be the case in ML FeSe on STO.

The calculations employ the Perdew-Burke-Ernzerhof (PBE) exchange-correlation functional [21], which describes reasonably well the (Li,Fe)OHFeSe system [15]. Iron-based superconductors are typically moderately correlated materials, and correlation effects beyond PBE can thus be important. Hence, we have used the PBE + U approach [22] with $U = 0.5$ eV (taken from the literature [23]) for Fe 3d electrons. We have also considered larger U values up to 4.3 eV [24], but the qualitative results do not depend on the U used in the calculation (See below). The projected augmented wave potential method [25] is employed for Fe (4s, 3d) and Se (4s, 4p) electrons, as implemented in the VASP code [26]. Van der Waals interactions are included via the DFT + D2 method [27]. The wave functions are expanded in a plane wave basis up to a cutoff energy of 400 eV. The Brillouin zone of the supercell (see below) is sampled by a Monkhorst-Pack 4×4×5 k-point mesh. The electronic structure calculations are converged to 10^{-6} eV, whereas the atomic structures are relaxed until the forces are less than 0.01 eV/Å.

We use an 80-atom supercell with 16 formula units of LiOHFeSe. Figure 1 shows, as an example, (a) a perspective side view and (b) a top view of the $Li_{0.75}Fe_{0.25}$OHFeSe supercell where there are Fe atoms substituting Li atoms in the LiOH spacer (Fe_{Li}), but no Li vacancy (V_{Li}). In this study, up to six defects [i.e., 4 Fe_{Li} + 2 V_{Li}, or (Fe_{Li}/V_{Li}) = (4/2)] are considered. In principle, different occupations of the lattice sites by the defects can affect the calculated results.

We find, however, that the variation at a given defect mix (Fe_{Li}/V_{Li}) is less than 6.5 meV/1x1, which has negligible effect on the magnetic phases of the FeSe layers.

Being a transition metal compound, FeSe has several isostructural phases due to different magnetic ordering. Experimental determination of the stable phases for (Li,Fe)OHFeSe is, however, not yet carried out. Here, we select candidate phases for the FeSe layers based on known structures in similar compounds. These include the CO, BI, PA, and Neel checkerboard (NE) phases, which are the stable commensurate AFM phases in the FeSe-derived systems [28]. The CO phase has been considered theoretically in the FeSe-derived systems [29-32], including the possibility as the stable phase of $Li_{0.8}Fe_{0.2}$OHFeSe [15]; the BI phase is a higher-energy phase for FeSe but ground state for FeTe [30]; the PA phase has recently been proposed for FeSe and LiOHFeSe as a topological insulator (TI) [33]; and the NE phase has been studied for bulk FeSe, ML FeSe, and FeSe on STO [32,34,35]. Note that all these phases are AFM phases. Figures 2(a-c) show the magnetic ordering for the first three, but not for the NE phase because, according to the calculation, it has a significantly higher formation energy.

Our study will be centered on the defect physics, as real (Li,Fe)OH spacer often contains defects, not only Fe_{Li}, but also V_{Li}. By applying a gate voltage V_g, Li ions are injected from ionic liquid ($LiClO_4$/polyethylene oxide) to reduce the concentration of V_{Li}, denoted as [V_{Li}], which in turn increases the concentration of conduction electrons, as reported by experiments [12]. Once the V_{Li} is depleted, it has been suggested [12] that the injection of additional Li ions will displace Fe_{Li}. Such a process is schematically shown at the bottom of Fig. 3, along with the corresponding Li concentration, [Li]. The rest of Fig. 3, on the other hand, shows the total energy as a function of [Li] for the CO, BI, PA, and NE phases, respectively. There is a one-to-one correspondence between [Li] (the horizontal axis) and the amount of defects [in parentheses, (Fe_{Li}/V_{Li})]. At (Fe_{Li}/V_{Li}) = (4/1), the CO phase has lowest energy. At (Fe_{Li}/V_{Li}) = (4/0), in contrast, the BI phase has lowest energy. At (Fe_{Li}/V_{Li}) = (2/0), the CO phase again has lowest energy. At (Fe_{Li}/V_{Li}) = (0/0) at which the (Li,Fe)OH spacer layer becomes defect-free, however, the PA phase takes over to become ground state. Curves in Fig. 3 are smooth fit to the calculated data. Although only semi-quantitative, one may use them to deduce approximate phase boundaries, which are [Li] = 70, 81, and 97%, respectively.

The reentrance of the CO phase at [Li] = 81% can be understood in terms of a doping effect. To see this, Fig. 3 shows the nominal doping level due to electron donation from (Li,Fe)OH to FeSe, as a function of V_g. It reaches a maximum at (Fe_{Li}/V_{Li}) = (4/0), when all the V_{Li}'s are depleted. Figure 3 shows that higher electron doping makes the CO phase less stable, as its total energy curve, to a large extent, traces the (purple) electron doping curve. The system thus would like to find a way to lower its energy, and the insulating BI phase offers a solution. Further increasing V_g, however, causes the replacement of Fe_{Li} by Li_{Li}. Fe_{Li} is a donor; a reduction in [Fe_{Li}] effectively reduces electron doping. Hence, there is no longer the need for the BI phase, so the CO phase becomes stable again. At even higher V_g, electron doping vanishes, leading to the PA phase when (Fe_{Li}/V_{Li}) = (0/0).

Note that the metal-insulator transition between CO and BI is not a property of (Li,Fe)OHFeSe *per se*, but that of ML FeSe. To see this, we show in Fig. 4 the band structures for (a) and (d) (undoped) ML FeSe, (b) and (e) (0.25 electrons per Fe) or 0.25-doped ML FeSe, and (c) and (f) $Li_{0.75}Fe_{0.25}$OHFeSe with (Fe_{Li}/V_{Li}) = (4/0), whose doping density is the same as in (b) and (e). For the CO phases, the band structure of 0.25-doped ML FeSe in Fig. 4(b) inherits that of undoped ML FeSe in Fig. 4(a), while the band structure of $Li_{0.75}Fe_{0.25}$OHFeSe in Fig. 4(c) inherits that of 0.25-doped ML FeSe in Fig. 4(b), except a level splitting due to (Li,Fe)OH spacer. The most noticeable difference between the doped and undoped cases is that E_F in the formers is shifted up by about 0.15 eV. For the BI phases, in contrast, while undoped ML FeSe in Fig. 4(d) remains to be metallic, both 0.25-doped ML FeSe in Fig. 4(e) and $Li_{0.75}Fe_{0.25}$OHFeSe in Fig. 4(f) are gapped, E_g~66-90 meV. In other words, electronic properties of $Li_{0.75}Fe_{0.25}$OHFeSe closely resemble those of 0.25-doped ML FeSe. Energetics of the CO-to-BI transition is also similar: when undoped, the CO phase of ML FeSe is more stable by 46 meV/1x1 than the BI phase; with a 0.25 electron per Fe doping, the latter becomes more stable by 4 meV/1x1.

It is experimentally known that the BI phase is stable in FeTe. The reason is because electron doping stabilizes the phase by satisfying the nesting condition at different k-points [36,37] and by itinerant Te *p* electrons, which give rise to large next-next-nearest neighbor super-exchange interactions [30], as revealed by a Heisenberg J_1-J_2-J_3 model. The model was also applied to FeSe [28,30]. Here, we refit the model for FeSe using the magnetic CO, BI, PA, and NE phases (relevant to this study). Our (J_1, J_2, J_3) = (112 meV, 75 meV, 21 meV) are in good agreement

with those in Ref. [28]. Note that the biquadratic term used in Ref. [28] only gives rise to a constant energy shift for the four magnetic structures that we have studied. As such, it does not affect our fitting parameters. It happens that the parameters are sensitive to doping. In (Li,Fe)OHFeSe with (Fe_{Li}/V_{Li}) = (4/2), the parameters change to (J_1, J_2, J_3) = (80 meV, 60 meV, 19 meV). With (Fe_{Li}/V_{Li}) = (4/0), they change again to (J_1, J_2, J_3) = (9 meV, 27 meV, 12 meV). The J_1 and J_2 are significantly reduced from those in bulk, due to a combination of the presence of (Li,Fe)OH spacers and electron doping. The BI phase is more stable than the CO phase, when the condition $J_2/J_3 < 2$ is met [28,30]. From the above discussions, it is clear that electron doping stabilizes the BI phase, as the ratio is reduced from 3.16 at (Fe_{Li}/V_{Li}) = (4/2) (low doping) to 2.25 at (Fe_{Li}/V_{Li}) = (4/0) (high doping). As doped electron occupies antibonding states between Fe d and Se p orbitals, itinerant Se p electrons play a role [30,38]. However, this is not enough. Instead, the FeSe layer exhibits an unusually large spin-phonon coupling, leading to the formation of Fe-**Fe**-Fe double dimers. This can be seen in Fig. 2(d) where every 3 Fe atoms of the same spin (out of every 4 same-spin Fe) are grouped together by shortening their distances to each other around the central **Fe** to 2.45-2.50 Å, which are about 7.3% shorter than that in the unrelaxed structure of 2.67 Å. In accordance, there is an accumulation of electrons between double dimer Fe atoms, shown in Fig. 2(d). By counting the nominal charge for (Fe_{Li}/V_{Li}) = (4/0), we find exactly one electron per double dimer. A comparison of the solid and dashed (green) lines in Fig. 3 shows that the double-dimer formation is essential for stabilizing the BI phase in ML FeSe.

As discussed earlier, FeSe exhibits electronic correlation effect [23,24,39,40]. This effect may be accounted for by the inclusion of an U for Fe 3d orbitals, so results for our systems qualitatively agree with experiments. We have also considered U values up to 4.3 eV [24], but the qualitative results do not depend on the U used in the calculation (See Fig. 5). Without the U, on the other hand, the BI phase is not only high in energy, but is also a metal. Thus, the role of the U here is to lift the energy degeneracy near E_F. We also performed a more-advanced dynamics mean field theory (DMFT) study. Here, we use a self-consistent DFT+DMFT approach, as implemented in the ABINIT code [41], which is based on the projector augmented-wave method [25]. The model Hamiltonian in DMFT is constructed with the help of projected Wannier orbitals [42], and the Anderson impurity model is solved by the continuous time quantum Monte Carlo method [43]. During the repeatedly calculation loops of DFT and DMFT, the electronic

local density is updated. We use U = 5.0 eV for the Coulomb interaction and J = 0.8 eV for the Hund's coupling, which are the values used previously for Fe-based superconductors [39]. The internal energy in the DFT+DMFT is computed from the DMFT charge density and impurity Green's function. The DMFT study requires a substantially larger computational resource, which limits the size of the system to be studied. Here, to examine the relative stability between the BI and CO phases, we used doped ML FeSe in vacuum, rather than the FeSe/(Li,Fe)OH superlattice. Table 1 shows the general trend of the energy change $\Delta E = E_{BI} - E_{CO}$ for both PBE+U and DMFT as a function of the doping. In spite that we have some technical difficulties in converging all the calculations, the general trend is clear, namely, DMFT lows the energy of the BI phase relative to the CO phase when the doping level is increased. Also, the BI phase in DMFT calculation is insulating for 0.5 e/Fe doping. In other words, the PBE+U, DMFT, and experimental results are all in agreement.

We should note that the relative stability of the BI phase is system dependent. For example, the BI phases in $Li_{0.75}Fe_{0.25}$OHFeSe and 0.25-doped ML FeSe are more stable than the corresponding CO phases by 20 and 4 meV/1x1, respectively. In 0.25-doped bulk FeSe, on the other hand, the BI phase is higher in energy than the CO phase by 22 meV/1x1; an even higher doping level of 0.5 electron per Fe is thus required to stabilize it. This explains why in bulk FeSe insulating phase only exists in high-doping regime over the superconducting dome [19], but in $Li_{0.75}Fe_{0.25}$OHFeSe it appears below or at the optimal doping level [12]. For ML FeSe on STO, however, experimental evidence of the BI phase is not yet available. As discussed in Ref. [44], the ML FeSe strongly binds to STO substrate. As such, the formation of Fe-**Fe**-Fe double dimers may be prohibited, which prevents the formation of insulating BI phase.

From the above, we may better understand the superconducting physics of (Li,Fe)OHFeSe. First, there should be a limit on the increase of T_C due to the formation of the insulating BI phase. It is noted that spin fluctuation near the transition to the BI phase may enhance the superconductivity, provided that the free-carrier concentration remains high. The formation of the insulating BI phase, however, eliminates the free carriers, whereby putting an upper bound to the increase of T_C. Indeed, in experiments [12], T_C increases with electron doping but transitions into an insulating phase at T_C = 43K. Second, our results suggest that one should avoid replacing substitutional iron, Fe_{Li}, by Li_{Li}, as this would decrease, rather than increasing, electron doping. Also, replacing Fe_{Li} by Li_{Li} is kinetically much harder than filling up Li vacancies, V_{Li}.

The most relevant question is, perhaps, how high the T_C can go if insulating BI phase can be suppressed? While what is the electron pairing mechanism for FeSe is still under debate, recent theories have proposed a phonon-mediated pairing mechanism for ML FeSe [34] and ML FeSe on STO [8-10]. Using the McMillan equation [45]: $T_C = \frac{T_D}{1.45}\mathrm{Exp}\left[\frac{-1.04(1+\lambda)}{\lambda-\mu^*(1+0.62\lambda)}\right]$, where T_D is the Debye temperature, μ^* is the repulsive Coulomb interaction, $\lambda \sim \rho V \gg \mu^*$, and ρ is the density of states at Fermi level, we can estimate T_C without knowing the exact origin of V, which, for simplicity, is assumed to be system independent. If we further denote $\xi = \rho/\rho^B$ as the DOS enhancement factor, where the superscript B denotes bulk FeSe, then

$$(T_C)^{\xi} = T_C^B\left[\frac{T_D}{1.45}e^{-1.04/(1-0.62\mu^*)}\right]^{\xi-1}. \quad (1)$$

In the case of (Fe_{Li}/V_{Li}) = (4/1), we find $\xi = 4.1$. Using $T_D = 230$ K, $\mu^* = 0.1$, which are in the range of previously calculated values [46-48], and Eq. (1), we obtain T_C = 33 K, which is smaller than the experimental value of 43 K [11,12]. The difference here may result from the ambiguity of input parameters. For example, as discussed in Ref. [9], interfacial high frequency phonon mode can enhance T_D. If we assume the interfacial phonon from (Li,Fe)OH spacer increases T_D to 350 K, then T_C = 45 K, which becomes similar to experiments. If we further increase ξ by doping without the formation the BI phase, T_C can increase to 79 K.

In summary, electronic and magnetic properties of FeSe systems over a wide range of doping level are studied by first-principles. It is found that high carrier concentration could destabilize the collinear phase through correlation interactions and subsequent structural relaxations in favor of an insulating bicollinear phase, which limits the further increase of superconducting temperature. One may avoid the transition to the bicollinear phase by increasing the bonding of the FeSe layer to its neighboring layer, but to further increase T_C also requires the increase of the Debby temperature T_D, as might be the case in ML FeSe on STO.

We thank Prof. X. H. Chen for stimulating discussions. Work at RPI was supported by the US Department of Energy under Grant No. DE-SC0002623. Work at KBSI was supported by Basic Science Research Program through the National Research Foundation of Korea (NRF) (NRF-2015R1C1A1A02037024) and KBSI grant D38614. Work at KAIST was supported by Basic Science Research Program through NRF (2014R1A1A2057202). The supercomputer time was

provided by National Energy Research Scientific Computing Center (NERSC) under DOE Contract No. DE-AC02-05CH11231 and the Center for Computational Innovations (CCI) at RPI.

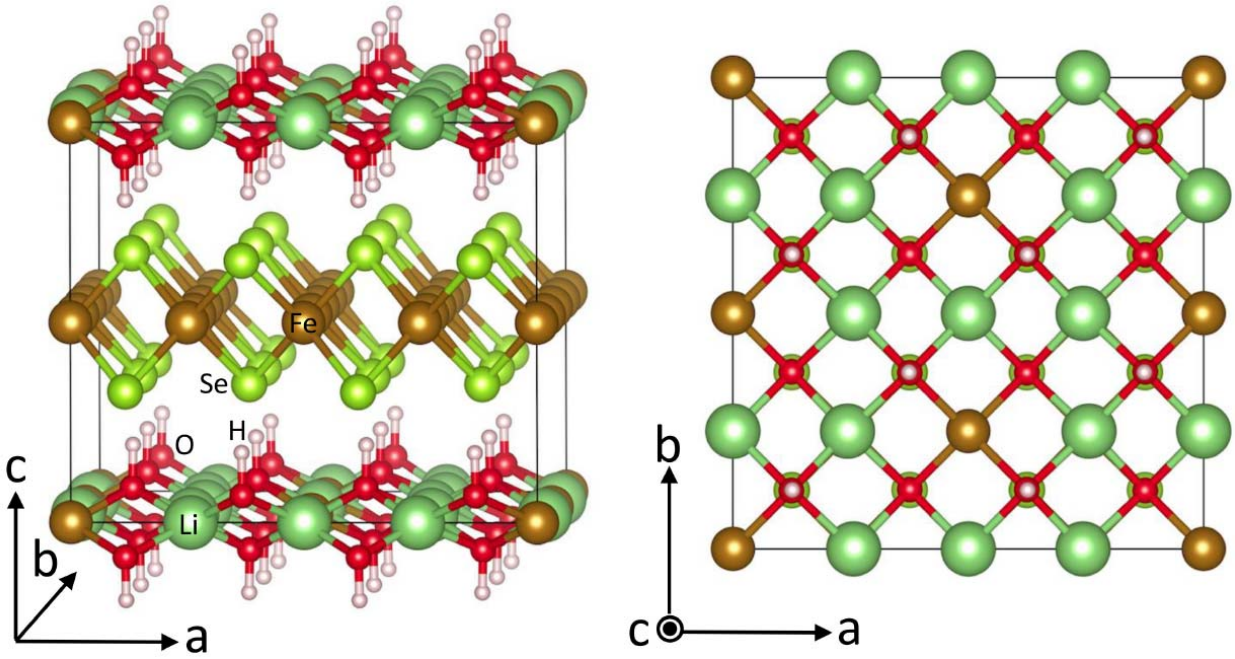

Figure 1. (a) Side and (b) top views of the supercell used in the calculation of (Li,Fe)OHFeSe, where brown, green, dark green, red, and pink balls are the Fe, Se, Li, O, and H atoms, respectively.

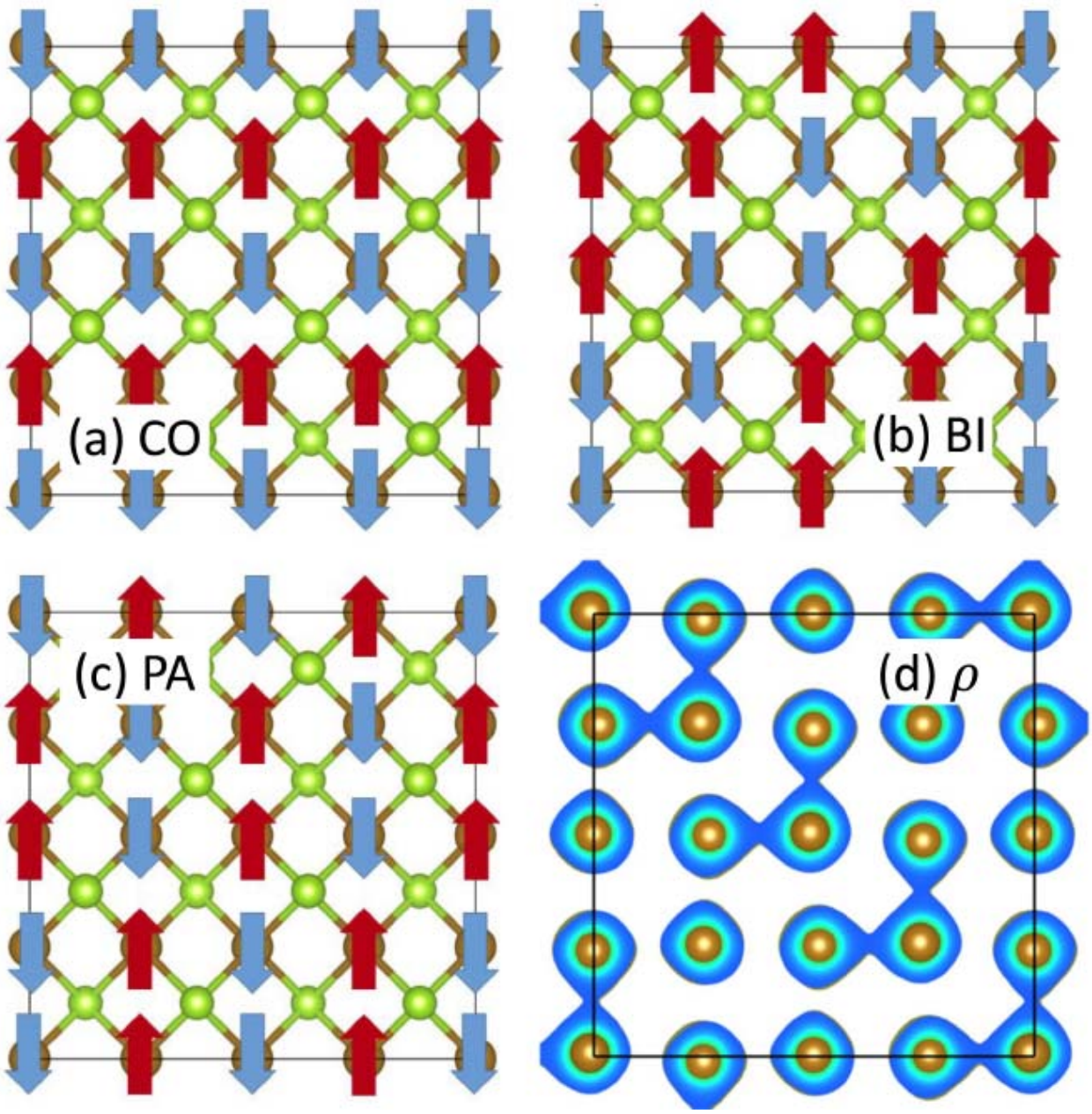

Figure 2. Spin texture of the (a) CO, (b) BI, and (c) PA phases. (d) Cross section of the total charge density ρ in the Fe plane for the BI phase. Fe double-dimers are clearly visible in the plot.

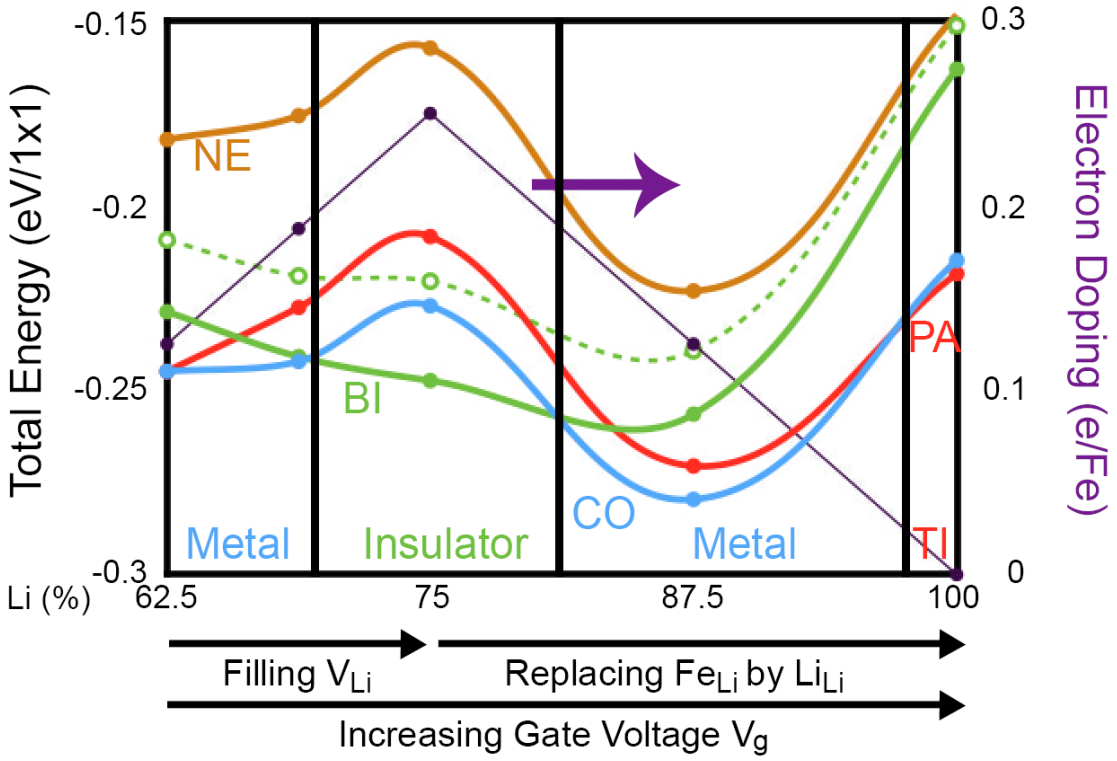

Figure 3. (Bottom) A schematic illustration of the effects due to applied gate voltage. (Li,Fe)OHFeSe is known to contain Li vacancies in the spacer. Increasing gate voltage first fills up the vacancies by Li ions, but then it replaces irons on the Li sites. (Top) Energy diagram of magnetically-ordered CO, BI, PA, and NE phases. Open circles connected by dashed line is for the BI phase without atomic relaxation. Vertical lines indicate the phase boundaries. Number pairs in the parentheses denote (Fe_{Li}/V_{Li}) in the supercell. The corresponding [Li] in the spacer is given near the bottom. The number of electrons donated by the spacer to the FeSe layer is also indicated (using the scale to the right).

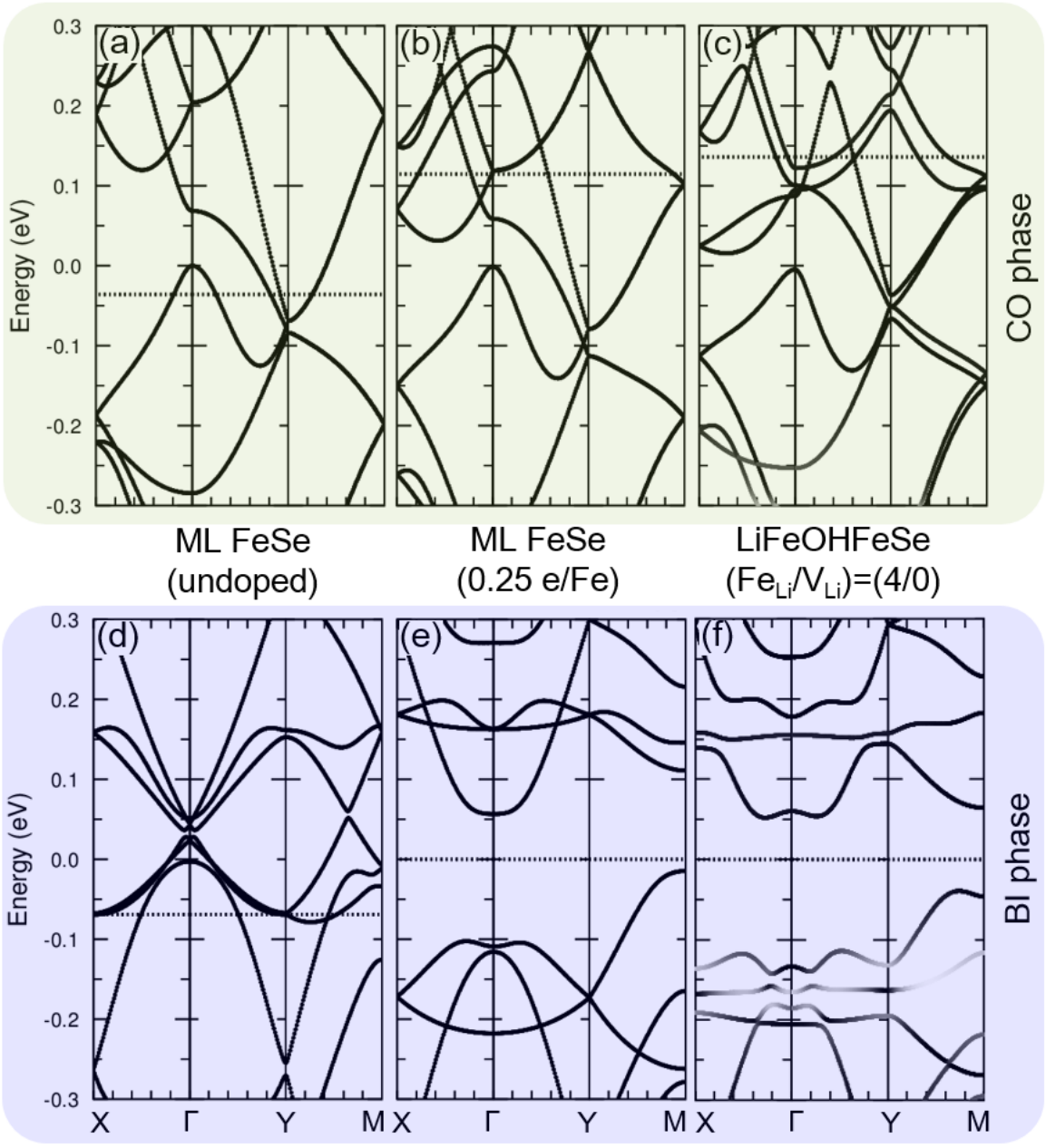

Figure 4. Band structures of (a-c) CO and (d-f) BI phases, respectively. (a) and (d) Undoped ML FeSe, and (b) and (e) (0.25 electrons per Fe)-doped ML FeSe, and (c) and (f) $Li_{0.75}Fe_{0.25}OHFeSe$ [with (Fe_{Li}/V_{Li}) = (4/0)]. Horizontal dotted lines denote E_F positions. While bands for the same chemical system are naturally aligned, between different systems, they are aligned according to deep Se *s* bands. Each state in (c) and (f) is projected onto the FeSe layer. The larger the projection, the darker the dot used for that state.

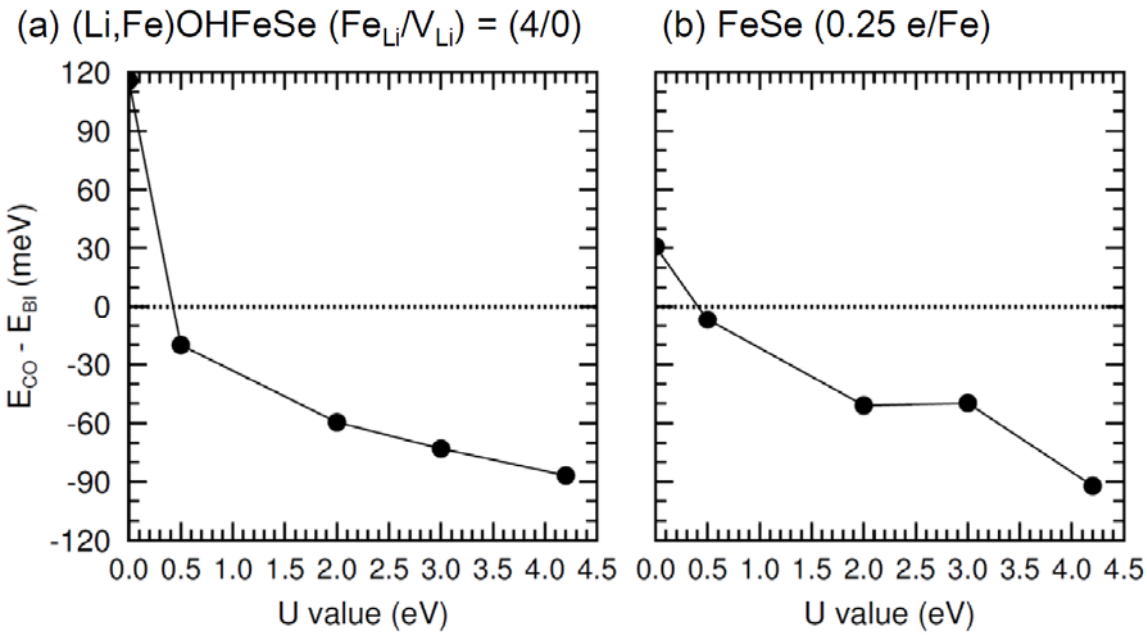

Figure 5. The enerngy difference between CO and BI phases with respect to the U value used in the PBE+U calculation for (a) (Li,Fe)OHFeSe (Fe_{Li}/V_{Li}) = (4/2) and (b) 0.25-electron doped FeSe. For U > 0.5 eV, the BI phase becomes stable in both systems.

Table 1. Energy difference between BI and Co phases ($\Delta E = E_{BI} - E_{CO}$) as a function of the doping for both PBE+U and DMFT (NC = Not converged).

Doping (e/Fe)		0	0.125	0.25	0.375	0.5
ΔE (meV/1x1)	PBE+U	47	26	-4	-33	-87
	DMFT	22	6.5	NC	NC	-330

References

[1] Y. Kamihara, H. Hiramatsu, M. Hirano, R. Kawamura, H. Yanagi, T. Kamiya, and H. Hosono, J. Am. Chem. Soc. **128**, 10012 (2006).

[2] Y. Mizuguchi, F. Tomioka, S. Tsuda, T. Yamaguchi, and Y. Takano, Appl. Phys. Lett. **93**, 152505 (2008).

[3] J.-F. Ge, Z.-L. Liu, C. Liu, C.-L. Gao, D. Qian, Q.-K. Xue, Y. Liu, and J.-F. Jia, Nat. Mater. **14**, 285 (2015).

[4] W. Li, H. Ding, P. Deng, K. Chang, C. Song, K. He, L. Wang, X. Ma, J.-P. Hu, X. Chen, and Q.-K. Xue, Nat. Phys. **8**, 126 (2012).

[5] F. Ming-Hu, W. Hang-Dong, D. Chi-Heng, L. Zu-Juan, F. Chun-Mu, C. Jian, and H. Q. Yuan, Europhys. Lett. **94**, 27009 (2011).

[6] S. Medvedevm, T. M. McQueen, I. A. Troyan, T. Palasyuk, M. I. Eremets, R. J. Cava, S. Naghavi, F. Casper, V. Ksenofontov, G. Wortmann, and C. Felser, Nat. Mater. **8**, 630 (2009).

[7] J. J. Lee, F. T. Schmitt, R. G. Moore, S. Johnston, Y. T. Cui, W. Li, M. Yi, Z. K. Liu, M. Hashimoto, Y. Zhang, D. H. Lu, T. P. Devereaux, D. H. Lee, and Z. X. Shen, Nature **515**, 245 (2014).

[8] Y.-Y. Xiang, F. Wang, D. Wang, Q.-H. Wang, and D.-H. Lee, Phys. Rev. B **86**, 134508 (2012).

[9] S. Zhang, J. Guan, X. Jia, B. Liu, W. Wang, F. Li, L. Wang, X. Ma, Q. Xue, J. Zhang, E. W. Plummer, X. Zhu, and J. Guo, Phys. Rev. B **94**, 081116 (2016).

[10] W. H. Zhang, X. Liu, C. H. P. Wen, R. Peng, S. Y. Tan, B. P. Xie, T. Zhang, and D. L. Feng, Nano Lett. **16**, 1969 (2016).

[11] X. F. Lu, N. Z. Wang, H. Wu, Y. P. Wu, D. Zhao, X. Z. Zeng, X. G. Luo, T. Wu, W. Bao, G. H. Zhang, F. Q. Huang, Q. Z. Huang, and X. H. Chen, Nat. Mater. **14**, 325 (2015).

[12] B. Lei, Z. J. Xiang, X. F. Lu, N. Z. Wang, J. R. Chang, C. Shang, A. M. Zhang, Q. M. Zhang, X. G. Luo, T. Wu, Z. Sun, and X. H. Chen, Phys. Rev. B **93**, 060501 (2016) (R).

[13] U. Pachmayr, F. Nitsche, H. Luetkens, S. Kamusella, F. Brückner, R. Sarkar, H.-H. Klauss, and D. Johrendt, Angew. Chem. Int. Ed. **54**, 293 (2015).

[14] X. H. Niu, R. Peng, H. C. Xu, Y. J. Yan, J. Jiang, D. F. Xu, T. L. Yu, Q. Song, Z. C. Huang, Y. X. Wang, B. P. Xie, X. F. Lu, N. Z. Wang, X. H. Chen, Z. Sun, and D. L. Feng, Phys. Rev. B **92**, 060504 (2015).

[15] W. Chen, C. Zeng, E. Kaxiras, and Z. Zhang, Phys. Rev. B **93**, 064517 (2016).

[16] L. Zhao, A. Liang, D. Yuan, Y. Hu, D. Liu, J. Huang, S. He, B. Shen, Y. Xu, X. Liu, L. Yu, G. Liu, H. Zhou, Y. Huang, X. Dong, F. Zhou, K. Liu, Z. Lu, Z. Zhao, C. Chen, Z. Xu, and X. J. Zhou, Nat. Commun. **7**, 10608 (2016).

[17] Y. J. Yan, W. H. Zhang, M. Q. Ren, X. Liu, X. F. Lu, N. Z. Wang, X. H. Niu, Q. Fan, J. Miao, R. Tao, B. P. Xie, X. H. Chen, T. Zhang, and D. L. Feng, Phys. Rev. B **94**, 134502 (2016).

[18] Z. Du, X. Yang, H. Lin, D. Fang, G. Du, J. Xing, H. Yang, X. Zhu, H. Wen., Nat. Commun. **7**, 10565 (2016).

[19] C. H. P. Wen, H. C. Xu, C. Chen, Z. C. Huang, X. Lou, Y. J. Pu, Q. Song, B. P. Xie, M. Abdel-Hafiez, D. A. Chareev, A. N. Vasiliev, R. Peng, and D. L. Feng, Nat. Commun. **7**, 10840 (2016).

[20] Y. Miyata, K. Nakayama, K. Sugawara, T. Sato, and T. Takahashi, Nat. Mater. **14**, 775 (2015).

[21] J. P. Perdew, K. Burke, and M. Ernzerhof, Phys. Rev. Lett. **77**, 3865 (1996).

[22] S. L. Dudarev, G. A. Botton, S. Y. Savrasov, C. J. Humphreys, and A. P. Sutton, Phys. Rev. B **57**, 1505 (1998).

[23] F. Zheng, Z. Wang, W. Kang, and P. Zhang, Sci. Rep. **3**, 2213 (2013).

[24] T. Miyake, K. Nakamura, R. Arita, and M. J. Imada, Phys. Soc. Jap. **79**, 044705 (2010).

[25] P. E. Blöchl, Phys. Rev. B **50**, 17953 (1994).

[26] G. Kresse, and J. Furthmüller, Comput. Mater. Sci. **6**, 15 (1996).

[27] S. J. Grimme, Comput. Chem. **27**, 1787 (2006).

[28] J. K. Glasbrenner, I. I. Mazin, H. O. Jeschke, P. J. Hirschfeld, R. M. Fernandes, and R. Valentí, Nat. Phys. **11**, 953 (2015).

[29] A. Subedi, L. Zhang, D. J. Singh, M. H. Du, Phys. Rev. B **78**, 134514 (2008).

[30] F. Ma, W. Ji, J. Hu, Z.-Y. Lu, and T. Xiang, Phys. Rev. Lett. **102**, 177003 (2009).

[31] K. Liu, Z.-Y. Lu, and T. Xiang, Phys. Rev. B **85**, 235123 (2012).

[32] B. Timur and M. L. Cohen, J. Phys.: Condens. Matter. **25**, 105506 (2013).

[33] H.-Y. Cao, S. Chen, H. Xiang, and X.-G. Gong, Phys. Rev. B **91**, 020504 (2015).

[34] T. Bazhirov, M. L. Cohen, Phys. Rev. B **86**, 134517 (2012).

[35] S. Coh, M. L. Cohen, and S. G. Louie, New. J. Phys. **17**, 073027 (2015).

[36] M. J. Han and S. Y. Savrasov, Phys. Rev. Lett. **103**, 067001 (2009).

[37] M. J. Han and S. Y. Savrasov, Phys. Rev. Lett. **104**, 099702 (2010).

[38] X.-W. Yan, M. Gao, Z.-Y. Lu, and T. Xiang, Phys. Rev. B **84**, 054502 (2011).

[39] Z. P. Yin, K. Haule, and G. Kotliar, Nat. Mater. **10**, 932 (2011).

[40] M. Aichhorn, S. Biermann, T. Miyake, A. Georges, and M. Imada, Phys. Rev. B **82**, 064504 (2010).

[41] X. Gonze *et al.* Comput. Phys. Commun. **205**, 106 (2016)

[42] B. Amadon, F. Lechermann, A. Georges, F. Jollet, T. O. Wehling, and A. I. Lichtenstein, Phys. Rev. B **77**, 205112 (2008)

[43] P. Werner, A. Comanac, L. de'Medici, M. Troyer, and A. J. Millis, Phys. Rev. Lett. **97**, 076405 (2006)

[44] J. Bang, Z. Li, Y. Y. Sun, A. Samanta, Y. Y. Zhang, W. Zhang, L. Wang, X. Chen, X. Ma, Q. K. Xue, and S. B. Zhang, Phys. Rev. B **87**, 220503 (2013).

[45] W. L. McMillan, Phys. Rev. **167**, 331 (1968).

[46] V. Ksenofontov, G. Wortmann, A. I. Chumakov, T. Gasi, S. Medvedev, T. M. McQueen, R. J. Cava, and C. Felser, Phys. Rev. B **81**, 184510 (2010).

[47] J. T. Peltonen, J. T. Muhonen, M. Meschke, N. B. Kopnin, J. P. Pekola, Phys. Rev. B **84**, 220502 (2011).

[48] J. Y. Lin, Y. S. Hsieh, D. A. Chareev, A. N. Vasiliev, Y. Parsons, and H. D. Yang, Phys. Rev. B **84**, 220507 (2011).